On single bubble mass transfer in a volatile liquid

Damien Colombet, Dominique Legendre, U. Tuttlies, Arnaud Cockx, Pascal Guiraud, U. Nieken, S. Galinat, C. Daniel

On single bubble mass transfer in a volatile liquid

D. Colombet [a,b,c,d,*], D. Legendre [a,c], U. Tuttlies [e], A. Cockx [b,c], P. Guiraud [b,c], U. Nieken [e], S. Galinat [d], C. Daniel [d]

[a] Institut de Mécanique des Fluides de Toulouse, IMFT, Université de Toulouse, CNRS, Toulouse, France
[b] LISBP, Université de Toulouse, INSA, INRA, CNRS, Toulouse, France
[c] Fédération de recherche FERMAT, CNRS, Toulouse, France
[d] Solvay R&I, 85, Avenue des Frères Perret, BP 62, 69192 Saint Fons, France
[e] Institut für Chemische Verfahrenstechnik Universität Stuttgart, Böblinger Str. 78, 70199 Stuttgart, Germany

Keywords:
Bubble
Fluid mechanics
Mass transfer

A B S T R A C T

We consider single bubble mass transfer of an non condensible gas into a volatile liquid phase in indus trial conditions, as observed for example in hydrocarbons liquid phase oxidation processes. Instantaneous bubble size, shape and velocity are measured using image processing with a particle tracking method. The mass transfer rate nitrogen into hot and pressurized liquid cyclohexane is deduced from the bubble volume decrease rate and is compared to literature correlations valid under isothermal conditions. Experiments are performed in a pressurized reactor for $P = 20$ bar, $30^\circ \leqslant T \leqslant 150\,^\circ$C and bubble Reynolds number $Re = O(10\ \ 100)$. The analysis of bubble rise dynamics shows that the gas liquid sys tem studied can be considered as a clean system. The mass transfer results are found to follow isothermal correlations predictions excepted for ambient temperature for which liquid evaporation in bubbles is shown to be coupled with mass transfer. This phenomena seems to be a consequence of having a high Lewis number.

1. Introduction

Bubbly flows are commonly used in chemical industries for the production of basic chemicals from hydrocarbons liquid phase oxi dation such as oxidation of p xylene (dimethyl ester), cumene (phenol, acetone), toluene (benzoic acid) or cyclohexane (cyclo hexanone, cyclohexanol). In that kind of applications, usually per formed in bubble columns or airlifts, gaseous oxygen transfers from bubbles to the liquid bulk where the hydrocarbon oxidation takes place at a temperature large enough to enable the chemical reaction (T 100 200 °C). Such elevated operating temperature condition requires to operate in pressurized bubble column to reduce evaporation of the liquid phase in the reactors. As a result, hydrocarbons liquid phase oxidation is usually conducted under moderate operating pressures (P 10 100 bar). In addition, to perform mass transfer and generate efficient species mixing in the liquid phase, reactors are often operated at very large gas flow rate with gas volume fraction often larger than 20%.

As pointed out recently by the detailed review of Rollbusch et al. [1], the amount of studies on bubbly flow *under pressurized conditions* is in fact to a small percentage of the whole literature on bubbly flow. In the last thirty years, the effect of increasing operating pressure on hydrodynamic and mass transfer of bubbly flows has been mainly investigated at the scale of a bubble column. For an air water bubbly flow in a bubble column, [2 4] found that the increase of operating pressure results in an increase of gas vol ume fraction for the same gas superficial velocity. The same behav ior is found by [5] for a nitrogen nheptane bubbly flow or by [6] for an air water/ethanol system. In the same time, [2] (air water) and [7] (nitrogen water and nitrogen cyclohexane) observed a decrease of the bubble size when increasing operating pressure. Mass transfer in pressurized reactor has been investigated at the scale of a bubble column using the sampling method in [3] or using optical oxygen probes in [4]. For similar gas superficial velocities, these works report an increase of the global mass transfer coeffi cient ($k_L a_l$) that results in both cases from the increase of gas vol ume fraction with operating pressure. The effect of increasing operating temperature on mass transfer in bubble column has been investigated by [8] for various organic liquids or by [9] for an air water system. Both works measured an increase of the global mass transfer coefficient that is attributed to the liquid phase properties variation with temperature and in particular to the increase of the mass diffusion coefficient of the solute. In those previous works, the study of the mass transfer was limited to the global mass trans

* Corresponding author at: LEGI, University Grenoble Alpes, France.
E-mail addresses: damien.colombet@legi.inp-grenoble.fr (D. Colombet), legendre@imft.fr (D. Legendre).

Nomenclature

Roman symbols

a	minor semi axis of the ellipsoid, m
b	major semi axis of the ellipsoid, m
c_{pL}	heat capacity of liquid phase at constant pressure, J kg^{-1} K^{-1}
C	nitrogen mass concentration in the liquid phase k, mg L^{-1}
C^I	saturation mass concentration, g L^{-1}
C_D	bubble drag coefficient
C_M	bubble added mass coefficient
C_L	bubble lift coefficient
d	bubble diameter, m
D	diffusion coefficient of nitrogen in liquid cyclohexane, m^2 s^{-1}
g	gravity constant, 9.81 m s^{-2}
H	bubble column height, m
He	Henry's constant for oxygen in water, Pa
J	surface average mass flux, kg s^{-1} m^{-2}
M_i	molar mass of species i, kg mol^{-1}
$m^G_{N_2}$	mass of nitrogen inside bubble, kg
P	operating pressure, Pa
P_G	pressure in gas phase, Pa
P^{sat}	saturation pressure of cyclohexane in gas phase, Pa
Pe	Péclet number based on the equivalent diameter and U (Pe $ReSc$)
Pe_{max}	Péclet number based on the equivalent diameter and U_{max} (Pe_{max} $(U_{max}/U)Pe$)
Sh	Sherwood number based on the equivalent diameter
r	bubble radius, m
Re	Reynolds number based on the equivalent diameter
S_b	bubble surface, m^2
Sc	Schmidt number (Sc ν_L/D_L)
T	operating temperature, °C
T^I	bubble surface average temperature, °C
t	time, s
U	bubble relative rise velocity, m s^{-1}
u_{max}	maximum liquid velocity at the bubble surface, m s^{-1}
V_b	bubble volume, m^3
x^k_i	molar fraction of specie i in phase k
y^k_i	mass fraction of specie i in phase k

Greek symbols

λ_k	thermal conductivity of phase k, W m^{-1} K^{-1}
μ_k	dynamic viscosity of phase k, Pa s
ν_k	kinematic viscosity of phase k, m^2 s^{-1}
ρ_k	density of phase k, kg m^{-3}
σ	surface tension, N m^{-1}
χ	aspect ratio (χ b/a)

Subscripts

G	gas phase
L	liquid phase

fer coefficient (k_La_l) because the bubble populations were usually polydispersed in size and non homogeneously distributed in the bubble column volume.

Recently, for an isothermal flow, the works of Colombet et al. [10,11] and Roghair et al. [12] on monodispersed dense homoge neous bubble swarms have shown that in the limit of high bubble Péclet number, the mass transfer in a dense bubbly flow can be described by using literature correlations dedicated to single bub ble for bubbly flows up to 30% of gas volume fraction. This partic ular behavior at high Péclet number is mainly due to a mass diffusion layer around bubbles much smaller than other character istic length scales of the flow at such Reynolds number.

Since the early 60s, it is known that bubble dynamics and mass transfer rate can be drastically influenced by the solutal Marangoni effect resulting from surface active contaminants accumulation at gas liquid bubble surface. For a clean system with no impurities or surfactant at the bubble surface, the terminal rise velocity of a spherical bubble can be accurately predicted by using the relation of Mei et al. [13]. For a fully contaminated surface, the terminal rise velocity of a spherical bubble can be determined with the correla tion established by Schiller and Nauman [14] for solid particle. As for mass transfer, with a clean interface system, mass transfer rate is usually based on the Higbie's penetration theory [15] with a con tact time defined as the ratio of the bubble diameter to the bubble rise velocity which is also known as the Boussinesq solution for a single spherical bubble [16]. Numerical simulations [17,18] have shown that this analytical solution appears to be very accurate to describe interfacial mass transfer for a single clean spherical bub ble rising in a still liquid, at large bubble Reynolds and Péclet num bers. Some corrections based on results for a single bubble have been introduced by Winnikow [19], Takemura and Yabe[17] or Colombet et al. [20] to account for the effect of a finite Reynolds number. For a fully contaminated bubble, the mass transfer rate can be described using the mass transfer relation established for a solid spherical particle [21 23]. For partially contaminated bub ble surface, bubble dynamic [24] and mass transfer [25,26] can be estimated from normalised drag coefficient proposed by Sadhal and Johnson [27] based on the stagnant cap model.

Since in oxidation processes the chemical reaction in liquid phase induced non isothermal flow conditions, it is presumed that some interactions may occure between the mass transfer of a solute and the phase change of the hydrocarbon liquid or vapor. In the literature, the study of gas/liquid transfer interaction with phase change has been mainly conducted for two different bubbly flow configurations: for bubble growth under boiling in the pres ence of non condensible gases and for bubble growth in supersat urated liquids. For boiling, at least since the 50's, it is admitted that dissolved gas interact with phase change mechanism affecting mainly the global heat transfer. It is shown from experimental studies that dissolved gas tend to increase the heat transfer coeffi cient compared to degassed liquids cases [28 30]. This enhance ment of global heat transfer can be attributed to a larger number of active nucleation sites especially for nucleate boiling conditions [30]. As a consequence, to get reproducible results when studying phase change in bubbly flows, it is necessary to control the non condensible gas concentration in the liquid phase and to degas the liquid if only phase change is studied. The dynamic of mass transfer in supersaturated liquid due to a rapid decompression has been studied by Payvar [31] or Bisperink and Prins [32] for des orption of carbon dioxide in liquids. By neglecting vapor pressure compared to noncondensible gas pressure in the bubble, Payvar found a good agreement with a model based on radi evolution from Rayleigh equation for the case of rising bubbles, while for the case of bubble growth from a cavity, Bisperink and Prins [32] found that applying the penetration theory to predict interfacial mass flux from Fick's law is sufficient to predict bubble growth rate. In both works where interaction of solute transfer and phase change should be present, the effect of the vapor pressure on the mass transfer is neglected. For the same application, Divinis et al. [33] have studied bubble growth in supersaturated solutions from

a fixed bubble formed on a micro heater in reduced gravity condition. The authors make the comparison between measured growth rate and predicted bubble growth from a model based on concentration and enthalpy conservation equations for a given bubble temperature. Their results seem to show that during the transfer, the bubble temperature decreases with time so that the transfer takes place in non isothermal conditions due to phase change. As a mater of fact, even if some previous studies have been conducted on the interaction betwen solute mass transfer and phase change for the particular case of boilling and gas desorption, one still suffer from a lack of knowledge of the mechanisms involved during bubbly flow mass transfer with the presence of phase change. To make progress on the subject, some new under standings are required.

Firstly, for process such as hydrocarbons liquid phase oxidation towers, it is of great interest to know if the gas liquid systems in industrial conditions can be considered as a clean system or rather as a contaminated system. Secondly, even if the operating pressure counterbalances liquid evaporation, in those process, a significant amount of vapor remains inside bubbles. As observed during this work and shown in Fig. 1, this liquid/vapor equilibrium may induce heat transfer around bubbles that can make very complex the description of mass transfer. An important issue is thus to know if mass transfer correlations cited above and established for isothermal conditions can directly be applied to the case of mass transfer in presence of a volatile liquid phase.

The objective of the present study is to investigate single bubble dynamics and mass transfer in presence of a volatile liquid phase for bubble Reynolds number in the range $Re \quad O(10 \quad 100)$. For this purpose, instantaneous measurements of bubble diameter, shape, rising velocity are first performed for the nitrogen cyclohexane gas liquid system at $P \quad 20$ bar and $30 \leqslant T \leqslant 150$ °C, with a vapor molar fraction in the bubble ranging from 0.8% to 27%. The mass transfer is analysed by measuring transfer rate from the bubble volume decrease.

The paper is organized as follows. Sections 2 describes the experimental set up. Section 3 presents results concerning bubble dynamic and mass transfer. Section 4 discuss mass transfer results regarding the effect of liquid evaporation into bubbles. Section 5 summarizes the main conclusions.

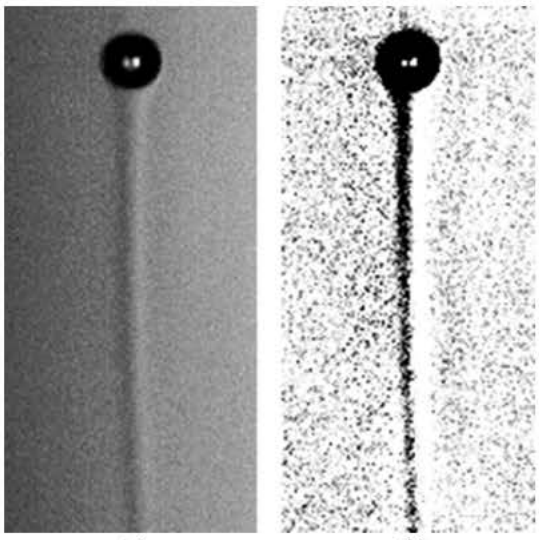

Fig. 1. Viewing of refractive index modification around bubbles thanks to an indirect lighting at $T \quad 150$ °C ($Re \approx 175$): (a) original image, (b) normalised image. This refractive index variation can have been either generated by a modification of liquid composition (nitrogen transfer) or temperature (cyclohexane evaporation/condensation) in the liquid phase.

2. Experimental set-up and instrumentation

In this section, the experimental installation is first described. Then, the experimental methods used for the determination of the bubble size, shape, velocity and mass transfer are presented.

2.1. Reactor design and gas liquid system

The bubble column used in this work has been previously developed and used by Schafer et al. [7,34] for the study of bubble size distribution and reaction kinetic of the cyclohexane liquid phase oxidation process. As depicted in Fig. 2a, the experimental set up consists in a one meter high stainless steel vessel with a square cross section equipped with 20 sapphire windows placed at five different levels. To better control bubble column geometry, a 90 mm high glass cylinder of 53 mm inner and 55 mm outer diameters is placed in the centre of the vessel. The vessel is filled with cyclohexane up to the fifth windows. As shown in Fig. 2b, bubbles are formed using a home made glass capillary of 12 cm length, 0.7 mm inner and 0.12 mm outer diameters. The glass cap illary is fixed and sealed by a PTFE tube on the gas injector duct. Two pressure regulators [PR] and a needle valve [NV] placed before the gas injection enable to control accurately the gas flow rate. Nitrogen bubbles are formed gently at the glass capillary tip and rise in the column. A small condenser is installed at the top of the column to condense any vapor present in the exhaust gas. Finally, the exhaust gas is burned by flowing on a Bunsen burner [B]. The vessel is pressurized using a secondary gas inlet at the upper flange [MF]. The pressure is controlled by a pressure regula tor placed on the exhaust gas line. If the pressure is higher than 50 bar a safety valve [SV], placed at the top flange, can open itself to evacuate the liquid in large water tanks. In addition, various check valves [CV] have been placed strategically on the installation to avoid any back flow. The vessel is heated up using two silicon oil heating circuits passing trough the vessel walls $[H_1, H_2]$. Before each experiment, the temperature homogeneity is checked using two thermocouples at the bottom and the top of the bubble col umn $[T_1, T_2]$. Experiments have been performed for a temperature difference smaller than 3 °C between lower and upper part of the bubble column for $T \quad 30, 50$ °C, and respectively smaller than 2 °C and 0.5 °C for $T \quad 100$ °C and 150 °C. In addition, between experiments, during each heating step, the gas inlet was stopped to prevent liquid saturation in nitrogen.

It is important to notice that present reported experiments under pressure and at elevated temperature have been performed with special care since, as any hydrocarbons, cyclohexane is highly flammable with a closed cup flash point of $\quad 20$ °C and a lower (resp. upper) flammability limit of 1.3% (resp. 8.4%) in volumetric percentage of air at ambient conditions. In addition, considering different previous industrial incidents, the mixture of cyclohexane hot vapor with oxygen is known to be explosive. For that reason, experiments were performed in a deflagration resistant vessel spe cially designed for the study of cyclohexane bubbly flows. More over, the bubble column was placed under a hood, in a continuously ventilated room equipped with cyclohexane vapor detectors.

2.2. Bubble size, shape and velocity measurements

The imaging set up consists of a high speed CCD camera (*PCO1200HS*, Fig. 2a) equipped with a fixed focal lens (Nikon macro 105 mm) and an extension ring (Nikon 27.5 mm) to visual ize a window of 19.2×15.3 mm located at the centre of the col umn at the level of the glass capillary tip. The spacial resolution is 66.6 px mm ^{1}. The camera is operated at 433 images per second

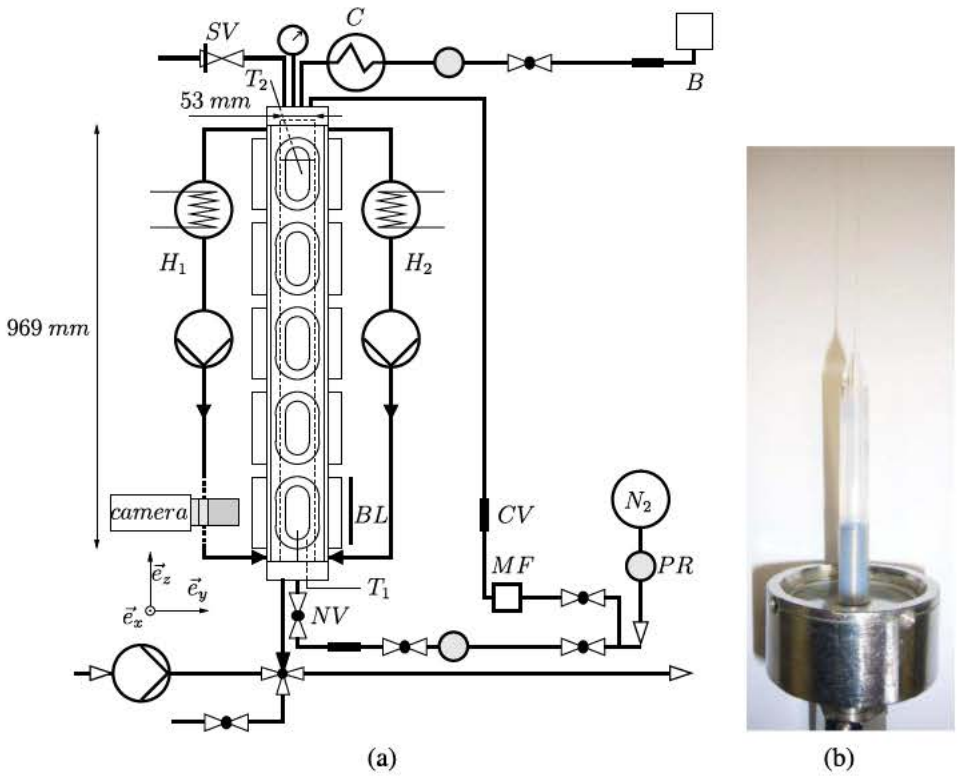

Fig. 2. (a) Experimental set-up (H heat exchanger, C condenser, MF mass flowcontroler, PR pressure regulator, B gas burner, T thermocouple, NV needle valve, CV check valve, SV safety valve, BL back lighting), (b) glass capillary injector.

with an exposure time of 0.3 ms. Lighting is supplied by diode backlight panels of 65,700 or 70,000 cd m ^{2} (*Phlox*).

Geometrical characteristics of bubbles such as the instanta neous major b and minor a semi axis, aspect ratio (χ b/a) and bubble rise velocity U have been measured using detection and tracking methods similar to those presented in Borchers and Eigenberger [35], Colombet et al. [10,11] and Bouche et al. [36]. The recorded images are processed by using *Matlab®*. The bubble edges are detected by applying a threshold to the grey level gradients of raw images. To insure the isotropy of gradient operator the gradient filter proposed by Marmottant and Viller maux [37] has been used. Examples of a tracked bubble are drawn on typical raw images in Fig. 3 for different times. As reported by Maxworthy et al. [38], with gas/liquid system having a low Morton number such as the present one (Mo $O(10^{11})$, note that even if bubble are slightly deformed their trajectories remain straight because as shown in Section 3.2 the bubble Weber number is lower than the critical value of $We_c \approx 2.30$ (Fig. 7b) that corresponds to the appearance of zig zag or spiral motion due to vortex shedding in bubble wake. In addition, using the relation proposed by Clift et al. [23] (p. 233), it has been checked that wall effects can be neglected in our experiments because bubble diameters are much smaller than bubble column diameter.

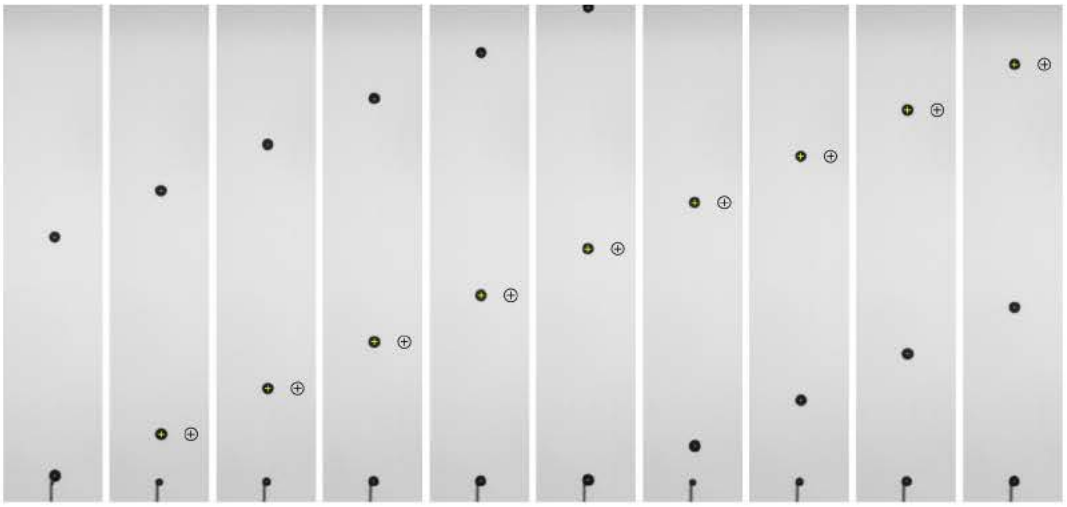

Fig. 3. Example of image processing applying particle tracking (T 30 °C,P 20 bar), shifted on the right side of the bubble: — bubble contour and + gravity center.

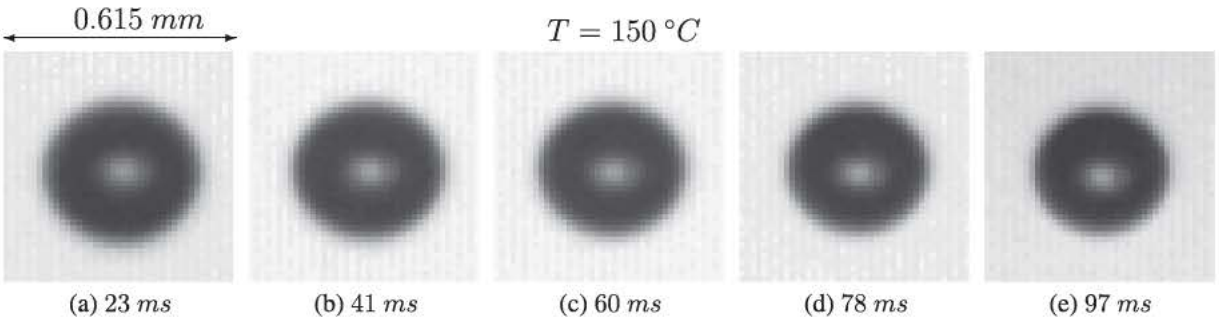

Fig. 4. Example of nitrogen gas bubble dissolution into cyclohexane at P 20 bar.

2.3. Mass transfer measurement

One objective of this work is to measure the mass transfer of nearly spherical bubbles rising and dissolving in liquid cyclohex ane. The mass transfer is here deduced from the decrease of the bubble diameter (see Fig. 4) as previously performed by Takemura and Yabe [17,25] and Vasconcelos et al. [39] under ambient condi tion. Prior to estimate the mass transfer, we discuss liquid/vapor equilibrium of cyclohexane, transfer equilibrium of nitrogen and bubble composition.

2.3.1. Nitrogen concentration at the bubble surface

For the considered binary system and operating conditions, the bubbles are composed of an non condensable gas: nitrogen (N_2) and a condensable gas: cyclohexane (RH). Thus, the mass transfer equilibrium of cyclohexane vapor in the bubble results from Raoult's law while the mass transfer equilibrium of nitrogen at the bubble surface results from Henry's law. Because of the low thickness of the gas liquid interface, those two equilibrium are ful filled at the bubble surface. According to Raoult's law, for the liq uid/vapor equilibrium, the cyclohexane vapor molar fraction in the gas phase x^G_{RH} can be given as x^G_{RH} $(\Phi P^{sat}/P_G)x^L_{RH} \approx \Phi P^{sat}/P_G$, where P^{sat} stands for the saturation pressure of cyclohexane that depends on the temperature. P_G is the gas phase pressure and $x^L_{RH} \approx 1$ is the liquid phase cyclohexane molar fraction. Φ is the fugacity coefficients ratio that takes into account the non ideality of the gas phase in Raoult's law and varies in the range $1.23 \leqslant \Phi \leqslant 1.3$. Thus, since we have a binary mixture (N_2, RH), assuming that liquid/vapor equilibrium is settled, the molar frac tion of nitrogen in the bubble $x^G_{N_2}$ is simply

$$x^G_{N_2} \quad 1 \quad x^G_{RH} \quad 1 \quad \frac{\Phi P^{sat}}{P_G} \tag{1}$$

The concentration jump at the interface of a noncondensible specie is given by Henry's law. Considering a low solubility of nitrogen in cyclohexane, Henry's law gives the relation between the nitrogen molar fraction in the gas phase $x^G_{N_2}$ and in the liquid phase $x^L_{N_2}$ at the bubble interface

$$x^L_{N_2} \quad \frac{P_G}{He} x^G_{N_2}, \tag{2}$$

where He (here in Pa) the Henry constant of nitrogen in cyclohexane is mainly depending on temperature. From Eq. (1), the molar frac tion jump is

$$x^L_{N_2} \quad \frac{P_G \quad \Phi P^{sat}}{He} \tag{3}$$

The nitrogen saturation mass concentration is related to the nitrogen molar fraction as

$$C^l \quad \rho_L \frac{M_{N_2}}{M_{RH}} x^L_{N_2} \quad \rho_L \frac{M_{N_2}}{M_{RH}} \frac{(P_G \quad \Phi P^{sat})}{He}, \tag{4}$$

with M_{N_2} and M_{RH} the molar mass of nitrogen and cyclohexane respectively. Note that some variations of the operating pressure has a direct effect on the saturation concentration since it modifies the gas phase pressure P_G. A variation of operating temperature also affect the saturation concentration by modifying the liquid cyclo hexane density (ρ_L $\rho_{L,RH}$). Moreover, the average temperature at the bubble surface T^l fixes the nitrogen Henry constant He and the vapor saturation pressure P^{sat}.

2.3.2. Vapor saturation inside the bubble

Dry gaseous nitrogen is injected through a glass capillary to form single bubbles in cyclohexane. Thus, during bubble formation, cyclohexane is flashed (fast evaporation) inside the bubble to fulfill Raoult liquid/vapor equilibrium. The question is to know if the bubbles are saturated or not with vapor at their departure. To clar ify this point from image processing we have measured the bubble formation time range t_{form} 0.2 0.3 s. The time required for filling the bubble with vapor has been estimated considering isothermal vapor mass transfer inside a fixed bubble of same departure diam eter as t_{sat} $0.416(d/2)^2/D_{G,RH} \approx 0.03$ s [20], where $D_{G,RH}$ is here the gas phase mass diffusion coefficient of cyclohexane in gaseous nitrogen. Thus, the time for isothermal vapor mass transfer inside bubble is found to be one order of magnitude smaller than the time required for the bubble formation. In addition, since evaporation process is usually faster than mass transfer process, it is also assumed in the following that bubbles are continuously vapor sat urated during their rise. In other words, liquid/vapor equilibrium is assumed to be reached inside the bubble at any time. Finally, the average temperature at the bubble surface is considered to stay close to the operating temperature thus $T^l \approx T$. Moreover, because of the both bubble size and the length of tracking (19.2 mm), Laplace pressure jump and hydrostatic pressure effect can be neglected in our experiment since both $\rho_L g(H \quad z)$ and $4\sigma/d$ are less than 1% smaller than the operating pressure. As a result, con sidering the system properties and operating conditions the molar fraction of nitrogen in the liquid phase lies between $x^L_{N_2}(P \quad 20$ bar$,T \quad 30\,^\circ$C$) \quad 1.5\%$ and $x^L_{N_2}(P \quad 20$ bar$,T \quad 150\,^\circ$C$)$ 1.7%. The saturation concentration in the liquid phase C^l (Eq. (4)) is calculated with the nitrogen Henry constant He and the vapor saturation pressure P^{sat} based on operating liquid bulk tempera ture T. To take into account compressibility effects, the gas phase densities of nitrogen and cyclohexane vapor are calculated consid ering the ideal gas law ($\rho_G \quad P_G M/(RT)$) valid for the operating pressure condition.

2.3.3. Duffusion coefficient of nitrogen into cyclohexane

The measurement of the Sherwood number requires the knowl edge of the diffusion coefficient of nitrogen into liquid cyclohex ane. In the literature, different relations can be found to estimate the mass diffusion coefficient of nitrogen in cyclohexane. To our knowledge, only one experimental work has tried to measure the diffusion coefficient of nitrogen in cyclohexane for a large temper ature range (19.8 141 °C). Using wetted sphere absorber method [40] the diffusion coefficients are found to be much larger than the prediction from usual correlations [41,42]. Due to the lack of a consensus on the diffusion coefficient of nitrogen in cyclohexane, the calculation of the diffusion coefficient is based here on the Stokes Einstein relation as

$$D_{N_2} \quad \frac{k_1 T}{k_2 \pi \mu_L \varsigma} \tag{5}$$

with the Boltzman constant k_1 1.381×10^{23} J K ^{1} and the nitro gen molecule diameter ς 3.749×10^{10} m. In this approach, the solute molecules are assimilated to spherical particles displacing in the liquid under thermal molecular motion so that k_2 3 (Stokes law). Note that using nuclear magnetic resonance method, for $3 < T < 114$ °C, Jonas et al. [43] have shown that Eq. (5) is able to describe the auto diffusion coefficient of cyclohexane with k_2 1.8. In this work, the original constant k_2 3 is considered.

2.3.4. Sherwood number calculation

Sherwood number is first determined from the bubble volume decrease considering only the mass balance of nitrogen at the scale of the bubble. The volume variation of the bubble due to the trans fer of nitrogen from gas to liquid can be describes from the concen tration difference at the bubble surface and in the liquid bulk (C^{l} $\langle C \rangle$) as follow

$$\frac{d(\rho_G V_b)}{dt} \quad \frac{dm_{G,N_2}}{dt} \quad \frac{\rho_G}{\rho_{G,N_2}} S_b k_L (C^{l} \quad \langle C \rangle) \tag{6}$$

where V_b $4\pi r^3/3$ and S_b $\pi 4r^2$ are respectively bubble instanta neous volume and surface, ρ_G and ρ_{G,N_2} are respectively gas mixture and gaseous nitrogen densities. The mass transfer coefficient k_L that is used to define the Sherwood number Sh $k_L d/D$ where D is the diffusion coefficient of nitrogen in the liquid phase and d $2r$ is the bubble diameter. By rearranging Eq. (6), the Sherwood number can be obtained from the time variation of bubble radius as

$$Sh \quad \frac{2r}{D} \frac{dr}{dt} \frac{\rho_{G,N_2}}{(C^{l} \quad \langle C \rangle)} \tag{7}$$

To measure the Sherwood number under isothermal condition, the same relation has been used by Takemura and Yabe [17,25] for oxygen dissolution in silicon oil and carbon dioxide mass transfer in water, respectively. Note that, since gas phase pressure variation are very small along the bubble path, gas densities variations with pressure can be neglected. Finally, since the gas inlet was closed during each step of operating pressure and temperature increase, the average concentration of nitrogen in the liquid phase is first assumed to stay close to the saturation concentration of nitrogen in liquid cyclohexane at storage conditions $\langle C \rangle (T$ 20°, P 1 bar) 0.14 kg m ^{3}.

3. Bubble dynamics

3.1. Bubble size and deformation

The time evolution of the bubble equivalent diameter deduced from the images is presented in Fig. 5 for the pressure P 20 bar and the four temperatures considered in the study

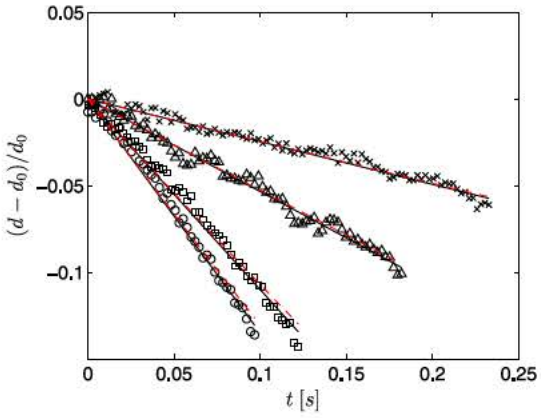

Fig. 5. Bubble equivalent diameter versus time for × T 30 °C, Δ T 50 °C, □ T 100 °C, ○ T 150 °C; — Eq. (8), – – Eq. (21).

T 30, 50, 100, 150 °C. The bubble diameter is normalized using the initial bubble diameter d_0. It is found to decrease with time for the four cases considered indicating that the dominant mecha nism is the transfer of nitrogen to the liquid. As shown in this fig ure, the bubble diameter is found to linearly decrease with time and can be described by

$$\frac{(d \quad d_0)}{d_0} \quad k_3 t, \tag{8}$$

with $k_3 (T$ 30 °C) 0.25 s ^{1}, $k_3 (T$ 50 °C) 0.53 s ^{1}, $k_3 (T$ 100 °C) 1.10 s ^{1}, $k_3 (T$ 150 °C) 1.35 s ^{1}.

This linear decrease is in agreement with the evolution observed by Takemura and Yabe [17,25] but it differs from the classical d^2 evolution of the form

$$d^2 \quad d_0^2 \quad k_4 t \tag{9}$$

observed for situations controlled by diffusion such as for example droplet evaporation. According to Eq. (7), relation (9) is obtained if the Sherwood number is constant while a linear evolution (Eq. (8)) should result from an evolution of the form $Sh \propto d$. In fact the lin earization of Eq. (9) gives $(d \quad d_0)/d_0 \approx k_4 t/2$ indicating that both evolutions are equivalent for small diameter reductions and then $k_4 \approx 2 k_3 d_0^2$. The decrease of bubble volume resulting from the nitro gen gas transfer to the liquid, the bubble diameter evolution is directly connected to the Sherwood number evolution (see Eq. (6)) where the bubble Péclet number is varying with both the bub ble diameter and velocity. Since the bubble velocity depends on its diameter a complex coupling between these parameters results in the bubble diameter evolution. These evolutions are addressed in the following and the time dependence of the bubble diameter will be clarified.

The instantaneous aspect ratio χ measured with the image pro cessing described in Section 2.2 is presented in Fig. 6. One can notice in this figure that for T 30 °C and 50 °C, the aspect ratio remains rather constant and close to unity ($\chi \leqslant 1.03$). For T 100 °C and 150 °C, bubbles are weakly deformed ($1.03 > \chi > 1.10$) with a maximum around $t \sim 0.02$ s correspond ing to the maximum in the bubble velocity. Then the bubble defor mation decreases due to the bubble volume decrease as it will be explained below. For present operating conditions, the Morton number Mo $g v_t^4 \rho_L^2 \Delta\rho / \sigma^3$ lies in the range $3 \times 10^{10} \leqslant Mo \leqslant 2 \times 10^{11}$. As shown by Legendre and Zenit [44] from exper imental measurements, the deformation of bubbles having a simi lar Morton number Mo $O(10^{10}$ $10^{11})$ and a constant volume is described by the following relation:

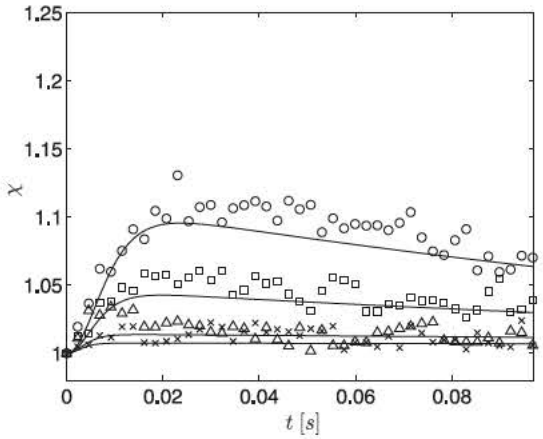

Fig. 6. Bubble aspect ratio versus time for × T 30 °C, Δ T 50 °C, □ T 100 °C, ○ T 150 °C; — aspect ratio using relation (10) with calculated Weber number.

$$\chi \quad \frac{1}{1 \quad \frac{9}{64}We} \tag{10}$$

Our experiments for bubbles with a time dependent diameter are compared with Eq. (10) in Fig. 6. Relation Eq. (10) is found to fairly reproduce the time variation of the bubble aspect ratio.

3.2. Bubble velocity

The evolution of the bubble velocity is reported in Fig. 8. The bubbles are tracked from their departure. As shown in this figure, the rise of a bubble presents two successive parts. First, under the action of buoyancy, the bubble accelerates to reach an almost constant rising velocity. The bubble deformation is here maximum. Then, the bubble begins to smoothly slow down due to the decrease of its volume (see Fig. 5). At large Reynolds number, the relaxation time of a bubble having a constant volume can be esti mated by $\tau_v \approx d^2/(72\nu_L)$ (this relation is obtained considering the added mass coefficient C_M 1/2 and the drag coefficient C_D 48/Re [45]). For $t \approx 5\tau_v$, the velocity of a bubble having a con stant volume is close to its terminal rising velocity. We have reported this characteristic time in Fig. 8 for each case. One can notice that the time t $5\tau_v$ describes the end of the first phase cor responding to the bubble acceleration. The corresponding instanta neous bubble Reynolds number Re Ud/ν_L and bubble Weber number We $\rho_L U^2 d/\sigma$ are presented in Fig. 7. As observed for the bubble velocity, both the Reynolds and Weber numbers varia tions follow two parts: first a fast increase up to their maximum value due to buoyancy and then a slow decrease due to the diam eter reduction. Because of the fluid properties evolutions with tem perature, the order of magnitude of the Reynolds and Weber numbers significantly varies with the temperature. After the bub ble acceleration phase, we observe the following orders of magni tude: $Re \approx 20$, 40, 100, 170 and $We \approx 0.04$, 0.09, 0.25, 0.5 for the temperatures T 30, 50, 100, 150 °C, respectively.

The trajectory of a bubble with volume variation can be described by the following force balance [46,47]:

$$\underbrace{C_M \rho_L V_b \frac{dU}{dt}}_{F_{AA}\ \text{Added mass acceleration}} \quad \underbrace{\rho_L V_b g}_{F_B\ \text{Buoyancy}} \quad \underbrace{2\pi\mu_L d f(Re) U}_{F_D\ \text{Drag}} \quad \underbrace{C_M \rho_L \frac{dV_b}{dt} U}_{F_{AV}\ \text{Added mass volume change}} \tag{11}$$

where C_M is the added mass coefficient and $f(Re)$ is a correction function of the drag coefficient defined as C_D $f(Re)16/Re$. The his tory force has been neglected because the bubble Reynolds number

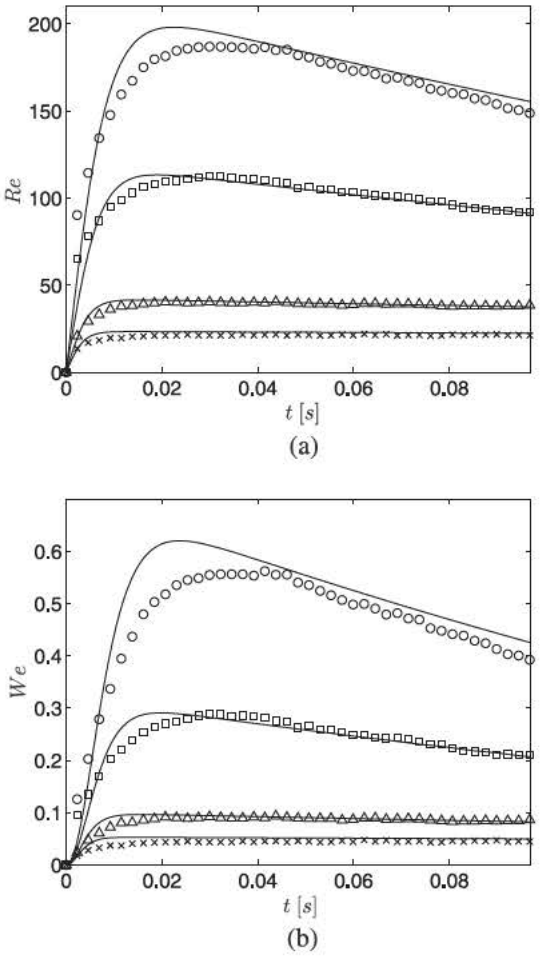

Fig. 7. (a) Bubble Reynolds number (Re Ud/ν_L) and (b) Weber number (We $\rho_L U^2 d/\sigma$) versus time for × T 30 °C, Δ T 50 °C, □ T 100 °C, ○ T 150 °C; — solving trajectory equation for a deformed bubble (Eqs. (11), (14), (15), (10)).

is much larger than unity [48]. For a spherical clean bubble, the drag correction can be accurately estimated using the relation proposed by Mei et al. [13]

$$f(Re) \quad \frac{16 + 3.315Re^{1/2} + 3Re}{16 + 3.315Re^{1/2} + Re} \tag{12}$$

while the added mass coefficient is

$$C_M \quad 1/2. \tag{13}$$

The effect of slight deformation on the drag and added mass forces can be considered using the following relations proposed by Moore [49] and Lamb [50], respectively:

$$f(Re) \quad 3G(\chi)\left(1 + \frac{H(\chi)}{Re^{1/2}}\right), \tag{14}$$

$$C_M \quad \frac{(1+e^2)(1 \quad e\cot{}^{1}e)}{1 \quad (1+e^2)(1 \quad e\cot{}^{1}e)} \qquad e \quad (\chi^2 \quad 1)^{1/2}, \tag{15}$$

with $G(\chi)$ and $H(\chi)$ functions of the bubble aspect ratio and given in [49]. Eq. (11) has been solved using an explicit 4th order Runge Kutta method considering both spherical bubbles (Eqs. (12) and (13)) and deformed bubbles (Eqs. (14) and (15)). The aspect ratio is calculated from Eq. (10) that fits experimental observations. As shown in Fig. 8, Eq. (11) clearly reproduces the two parts observed for the velocity evolution. For T 30 °C and T 50 °C, results for a spherical bubble ( ) are very close to those for a deformed bubble

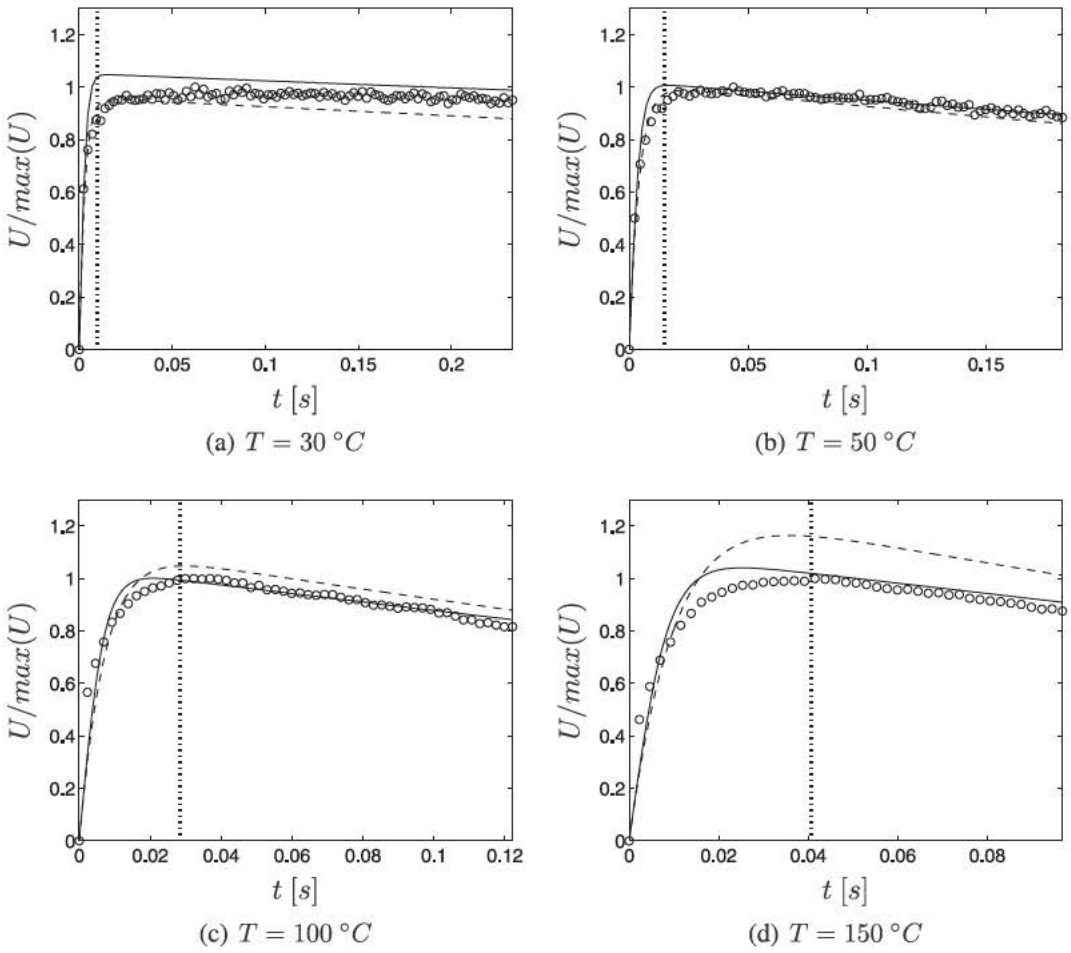

Fig. 8. Bubble velocity versus time: ○ Exp. P 20 bar, solving trajectory equation (Eq. (11)): –– for a spherical bubble with C_D from Mei et al. [13] (Eq. (12)) and C_M 1/2, – for a deformed bubble with C_D from Moore's relation [49] (Eq. (14)), C_M from Lamb [50] (Eq. (15)) and χ from Legendre and Zenit [44] (Eq. (10)), ... $5\tau_v$.

( ) since the aspect ratios remain close to unity ($\chi \approx 1$). For T 100 °C and T 150 °C, the bubbles are more significantly deformed ($1.03 > \chi > 1.10$) and the corrections (Eqs. (14) and (15)) taking into account the effect of the deformation improve the comparison. Such good agreement confirms that history force can be neglected in present situation.

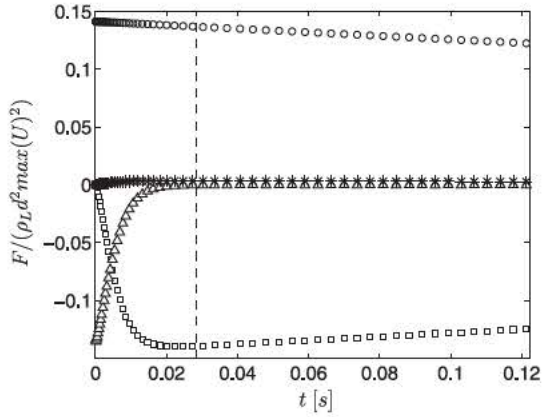

Fig. 9. Example of force balance variation versus time solving trajectory equation for a deformed bubble at T 100 °C : ○ F_B buoyancy force, □ F_D drag force, added mass force contributions: Δ F_{AA} bubble acceleration and ∗ F_{AV} bubble volume time variation, –– $5\tau_v$.

Fig. 9 reports the detail of the forces experienced by a bubble at T 100 °C. Initially, at bubble departure, the buoyancy force F_B is balanced by the added mass force F_{AA} induced by the bubble acceleration so that the bubble initial acceleration is $dU/dt \approx g/C_M$. Due to the bubble velocity increase, the drag force F_D increases up to a maximum when the bubble velocity is maximum. Then, due to the bubble volume decrease, the buoyancy force F_B slowly decreases. In the same time, added mass force due to acceleration gradually vanishes. The contribution of the added mass force F_{AV} induced by the bubble volume variation (last term in Eq. (11)) slightly increases the bubble velocity but its contribution remains very small compared to the over forces ($F_{AV}/F_B \approx 2$ 3%). For $t > 5\tau_v$, the buoyancy force almost balances the drag force ($F_B/|F_D| \approx 98\%$) resulting in a force balance similar to the case of a bubble of constant volume because the interfacial velocity $|dR/dt|$ is much smaller than the bubble rise velocity U [46]. For the present experiments (see Table 1), we have $|dR/dt|/U \approx 0.1$ 0.5% and a quasi static rise is then observed for all the considered cases. As a consequence, for $t > 5\tau_v$, it is possible to access directly to the drag coefficient considering in Eq. (11) only the balance between drag and buoyancy as

$$C_D \approx \frac{4}{3}\frac{\Delta\rho g d}{\rho_L U^2} \tag{16}$$

The corresponding drag coefficients deduced from our experiments are reported in Fig. 10 versus the Reynolds number for $t > 5\tau_v$. Experimental results are compared to the relation (12) (spherical

Table 1
Experimental characteristic times and dimensionless numbers for $t > 5\tau_v$ (except $*$: for the whole rising time).

T (°C)	τ_v (ms)	τ_D (ms)	Re	$\frac{dR/dt^*}{U}$	Sc	$Pe \times 10^3$	Pr	Pe^{th}	Le
30	1.9	31	20–22	0.07–0.10	720	14–16	12	240–264	60
50	3	25	34–41	0.15–0.27	382	13–16	10	340–410	38
100	5.9	19	84–111	0.20–0.35	105	9–12	7	588–777	15
150	8.4	17	156–196	0.20–0.43	39	6–7.6	6	936–1176	6.5

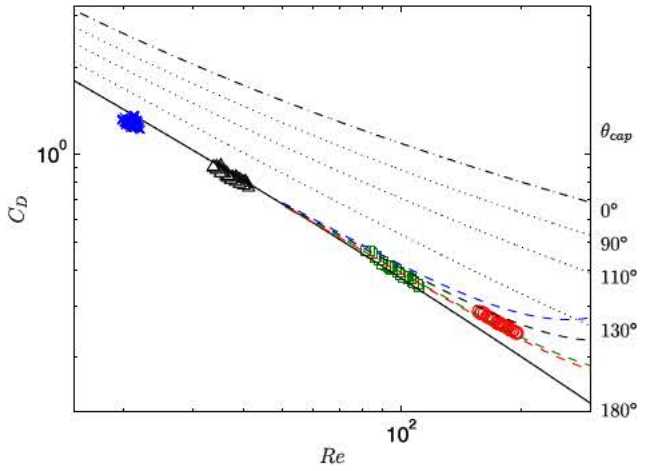

Fig. 10. Bubble drag coefficient versus Reynolds number for × T 30 °C, ΔT 50 °C, □ T 100 °C, ○ T 150 °C; — clean spherical bubble (Eq. (12), θ_{cap} 180°), -.- fully contaminated spherical bubble ([14], θ_{cap} 0°), . . .partially contaminated spherical bubble according to stagnant cap model with θ_{cap} 90 − 110 − 130°, −− clean deformed bubble (Eqs. (14) and (10)).

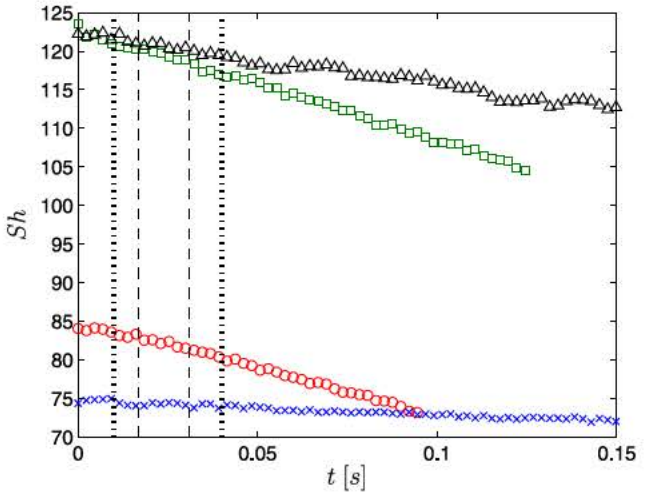

Fig. 11. Bubble sherwood number evolution versus time for × T 30 °C, ΔT 50 °C, □ T 100 °C, ○ T 150 °C, − − $\tau_D \approx 17$–$31\ ms$, . . . $5\tau_v$ 10–40 ms.

bubble), the relation (14) (slightly deformed clean bubble) and the relation of Shiller and Nauman [14] (fully contaminated spherical bubble). In addition, we have also reported in this figure the drag coefficient for a partially contaminated bubble using the normalized drag coefficient proposed by Sadhal and Johnson [27] with drag cor relations of Mei et al. [13] and Shiller and Nauman [14] as reference drag coefficients for clean and fully contaminated bubble, respec tively. A similar drag description for a partially contaminated bub ble at moderate Reynolds number has been previously validated by Takemura and Yabe [25] with experimental measurements and by Dani et al. [51] with numerical simulations. As shown in Fig. 10, the drag coefficient is closer to the evolution of a clean bubble than to the evolution of a contaminated bubble. For T 30 °C and 50 °C, experimental data are matching with correlation of Mei et al. [13], the bubbles being spherical. For T 100 °C and 150 °C, experimen tal drag coefficients are described by Moore's relation [49], the bub bles being weakly deformed. One important conclusion is that the gas/liquid system studied here (nitrogen/cyclohexane) is therefore a clean system. This behavior is mainly explained by the fact that cyclohexane molecules are non polar. Indeed, contrary to water, non polar impurities possibly present and dispersed in the liquid phase, do not accumulate preferentially at the bubble gas liquid interface, as observed for bubbles in silicon oil [17].

4. Nitrogen mass transfer

The nitrogen mass transfer at the bubble surface is determined using relation (7). Because of time fluctuation in the diameter mea surements (see Fig. 5), the estimation of the Sherwood number is performed considering the mean bubble volume decrease rate from Eq. (8) so that dr/dt $k_3 d_0/2$. The corresponding time evolution of the Sherwood number is reported in Fig. 11. We observed that the transfer decreases with the time due to the reduction of the bubble surface. Note that we do not observe different stage in the transfer. In fact, for a steady bubble rise, the time corresponding to the transient evolution of the mass transfer can be estimated considering the work of Figueroa and Legendre [18]. The time evo lution of the transfer of a ellipsoidal bubble suddenly released at its terminal velocity in a liquid at rest is reported for conditions close to the one considered in our study (Re 300, Sc 10 and χ 1.2). The mass transfer is shown to reach a steady state for a time larger than $\tau_D \approx 10/(U/(d_b^3\chi/8)^{1/3})$. For the experiments performed in this work, we get τ_D 17 31 ms so that mass transfer should be in steady state very shortly after the bubble departure from the capil lary. τ_D and $5\tau_v$ are reported in Fig. 11 and in Table 1. They have the same order of magnitude and for $t > \tau_D$ and $t > 5\tau_v$, a quasi steady state is reached for both bubble dynamic and mass transfer. The corresponding Sherwood numbers are plotted against the Reynolds number in Fig. 12. For the different experiments, the Sherwood number evolves between 55 (T 150 °C) and 119 (T 50 °C). One need to mention here that the reproducibility of the measure ments presented in Fig. 12 for one bubble has been checked for four consecutive bubbles.

It is now possible to compare our experimental results to the correlations from the literature. In most of studies on mass transfer in bubble columns, the rate of transfer is estimated by using the Higbie's penetration theory [15] where the contact time is defined as the ratio of the bubble diameter to the bubble rise velocity. The corresponding correlation is equivalent to the analytical solution obtained earlier by Boussinesq [16] by considering that the flow around the bubble can be approximated by the potential flow and that the transfer occurs across a very thin concentration layer at the bubble surface

$$Sh \quad \frac{2}{\sqrt{\pi}} Pe^{1/2}, \tag{17}$$

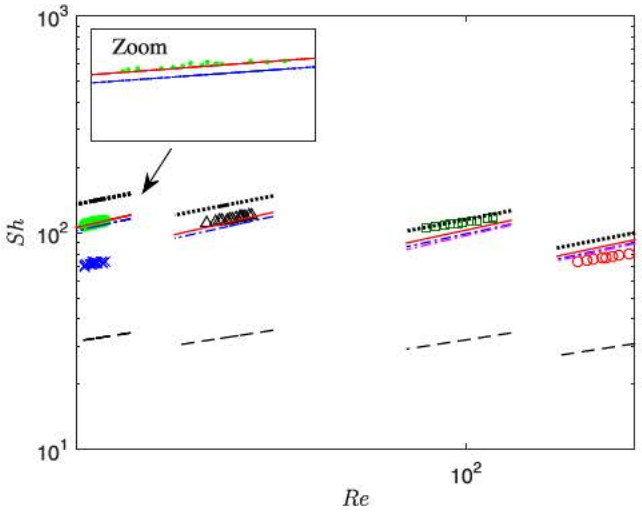

Fig. 12. Sherwood number (Eq. (7)) versus Reynolds number for × T 30 °C, Δ T 50 °C, □ T 100 °C, ○ T 150 °C; . . . solution of Boussinesq [16] Eq. (17); -.-.- Eq. (18) [19]; -.-.- Eq. (19) [17]; — Eq. (20) [20]; – – – Fully contaminated spherical bubble Eq. (22) [23]; • Eq. (24) with Ja 0.006 (ΔT 0.1 °C) and Nusselt number estimated from Eq. (25).

with the Péclet number Pe $ReSc$ where Sc ν_L/D is the Schmidt number of nitrogen in liquid cyclohexane. The corresponding values for both Pe and Sc are reported in Table 1. This relation is supposed to be valid in the limit of both large Re and Pe. Various improvements have been proposed to account for the effect of moderate Reynolds number and the effect of bubble deformation. Considering the flow approximation of Moore [52], Winnikow [19] derived the following expression valid for $Re > 50$ [18]

$$Sh \quad \frac{2}{\sqrt{\pi}}\left[1 \quad \frac{2.89}{\sqrt{Re}}\right]^{1/2} Pe^{1/2}. \tag{18}$$

Measuring the mass transfer of almost spherical millimeter sized bubbles from volume variations, Takemura and Yabe [17] proposed the following relation for $0.03 < Re < 100$ and $Pe \gg 1$,

$$Sh \quad \frac{2}{\sqrt{\pi}}\left[1 \quad \frac{2}{3}\frac{1}{(1+0.09Re^{2/3})^{3/4}}\right]^{1/2}(2.5+Pe^{1/2}) \tag{19}$$

which is in good agreement with both experiments and numerical simulations at moderate Re and large Pe. Relation (19) has been validated by direct numerical simulation up to Re 1000 [18]. Recently, Colombet et al. [20] showed that the relevant Péclet number for the description of the mass transfer at a clean interface is the Péclet number Pe_{max} based on the maximal velocity U_{max} $Uf(Re)/2$ of the liquid at the interface (Eq. (12), [53]) instead of the bubble rise velocity U. Based on this results the following relation is able to describe the mass transfer for a spherical bubble whatever the value of Re and Pe

$$Sh \quad 1+\left[1+\left(\frac{4}{3\pi}\right)^{2/3}(2\,Pe_{max})^{2/3}\right]^{3/4}, \tag{20}$$

When Pe_{max} tends to zero, relation (20) tends to the diffusive solution $Sh(Re \quad 0) \quad 2$ while it tends towards the Boussinesq solution (17) when Re and Pe become very large compared to unity. This relation is also in agreement with the experiments of Takemura and Yabe [17] and numerical simulations from various previous works [20].

These relations are reported in Fig. 12. For experiments with hot cyclohexane at T 50 °C, T 100 °C and T 150 °C, experimental measurements are fairly in agreement with relation (18) (20) dedicated to mass transfer under isothermal conditions. One can notice that relations (18) (20) give in fact very similar values for Sh. Since the Reynolds numbers are in the range 20 196, relation (17) [16] over predicts experimental results, as expected. The agreement with transfer under isothermal conditions suggests that the transfer is not affected by cyclohexane evaporation at the interface. The time variation of the bubble diameter can now be explained. First, since we get at first order $CD \propto 1/Re \propto 1/(Ud)$, the force balance show us that $U \propto d^2$ (Eq. (16)). Secondly, since we get at first order $Sh \propto Re^{1/2} \propto U^{1/2}d^{1/2}$, one can thus show that $Sh \propto d^{3/2}$. Then, the mass transfer balance at the bubble scale follows $Sh \propto$ $d\dot{d}$ (Eq. (7)) so that the expected evolution for the bubble diameter would be

$$d \quad d_0(1 \quad k_5\,t)^2 \tag{21}$$

The linearization of this relation recovers the experimental evolution given by Eq. (8) with k_5 $k_3/2$. As reported in Fig. 5 (red[1] dash line), a good agreement is found with Eq. (21).

However, for experiments closer to ambient temperature T 30 °C, the measured Sherwood number is found to be much lower than the prediction obtained with correlations mentioned above considering isothermal conditions. This strong underestimation of the Sherwood number is concomitant to the observation of a much lower bubble volume decrease rate (see symbols × in Fig. 5).

We have first checked as a possible explanation for the difference observed at T 30 °C, a possible effect of interface contamination. The drag evolution clearly show that experiments were conducted for mobile (clean) interfaces. To confirm this, we compare our results with the relation used for the description of the transfer at an immobile (fully contaminated) bubble surface [23]

$$Sh \quad 1+Sc^{1/3}Re^{0.41}\left(1+\frac{1}{Pe}\right)^{1/3} \tag{22}$$

Eq. (22) is valid for $1 \leqslant Re \leqslant 400$ and $0.25 \leqslant Sc \leqslant 100$. This relation is reported in Fig. 12 (dash lines) and is clearly far to describe the transfer. Both bubble dynamic (Fig. 10) and mass transfer measurements (Fig. 12) show that bubble surface is not contaminated. Discrepancy found for T 30 °C can not be explained by the bubble surface contamination.

The reason of the discrepancy found at T 30 °C is explained in the next section.

5. Discussion: on the evaporation effect on the mass transfer

In Section 2.3.2, we estimated that the bubbles are saturated in vapor at departure by calculating saturation time under isothermal conditions. If evaporation is present during the bubble formation we can not consider isothermal conditions and bubbles can not be considered as saturated with vapor at their departure. For non isothermal conditions, it is quite difficult to estimate the time required to reach vapor saturation since the bubble interface temperature during liquid evaporation is an unknown parameter. Thus our estimation of the saturation time corresponds to a lower limit of this time since the heat transfer from the liquid to the interface, required for evaporation, should increase the time necessary for saturation. So at lower temperature, evaporation is lower and we need to explore if the liquid phase is still evaporating in the bubble after departure.

To answer to this question, we consider that the bubble volume evolution is now controlled by both nitrogen gas/liquid mass trans

[1] For interpretation of color in 'Fig. 5', the reader is referred to the web version of this article.

fer and liquid/gas evaporation of cyclohexane at the bubble surface. To do that, we rewrite the bubble mass balance considering these two contributions. Eq. (7) is then corrected as follow

$$\frac{d(\rho_G V_b)}{dt} \quad \frac{\rho_G}{\rho_{G,N_2}} S_b k_L (C^l \quad \langle C \rangle) + \frac{\rho_G}{\rho_{G,vap}} \frac{S_b H_L}{L} (\langle T_L \rangle \quad T_L^l) \tag{23}$$

where T_L^l is the temperature of the liquid at the bubble surface and $\langle T_L \rangle$ the temperature in the bulk of the liquid phase. H_L is the heat transfer coefficient between the bubble and the liquid under phase change. L stands for the latent heat of evaporation of the liquid cyclohexane. The difficulty here is that T_L^l is unknown and can not be measured in the experiment. By introducing the heat conduction coefficient λ_L, the heat transfer coefficient is linked to the Nusselt number as $H_L \quad Nu\lambda_L/d$. For bubble phase change, the Nusselt number is usually calculated from the Jakob number $Ja \quad \rho_L C_{p_L}(\langle T_L \rangle \quad T_L^l)/(\rho_{G,vap} L)$ that compares the sensible heat in the liquid phase to the latent heat required for evaporation [54,55]. By rearranging Eq. (23), one can show that in presence of evaporation, the Sherwood number becomes

$$Sh \quad \left(LeNuJa \quad \frac{2r}{D} \frac{dr}{dt} \right) \frac{\rho_{G,N_2}}{(C^l \quad \langle C \rangle)} \tag{24}$$

where the Lewis number $Le \quad D_L^{th}/D$ compares heat diffusion to mass diffusion of a solute (nitrogen) in the liquid phase. Here, $D_L^{th} \quad \lambda_L/(\rho_L C_{pL})$ stands for the thermal diffusivity (heat diffusion coefficient) in the liquid phase. For $Ja \quad 0$ ($\Delta T \quad \langle T_L \rangle \quad T_L^l \quad 0$), Eq. (24) is equivalent to Eq. (7). In the same way, considering the absence of dissolved gas in the bubble (i.e. a pure vapor bubble), $Sh \quad 0$ and Eq. (24) reduces to the enthalpy balance induced by phase change as considered for the description of nucleate boiling. For the temperature range considered in this study, the thermal diffusivity of liquid cyclohexane decreases proportionally with the temperature so that $D^t h_L \propto T$ while the mass diffusion coefficient is proportional to the temperature divided by the dynamic viscosity $D \propto T/\mu_L$ (see Eq. (5)). As a result, the evolution of the Lewis number with the temperature is, at first order, very similar to the one of the dynamic viscosity $Le \propto \mu_L \propto 10^{cste/T}$. For the present experiments with cyclohexane (see Table 1), the Lewis number is found to significantly decrease with the temperature from $Le(T \quad 30\,^\circ\mathrm{C}) \quad 60$ to $Le(T \quad 150\,^\circ\mathrm{C}) \quad 6.5$. There is on order of difference between $T \quad 30\,^\circ\mathrm{C}$ and $T \quad 150\,^\circ\mathrm{C}$. This behavior can explain why for $T \quad 30^\circ$ experimental results for Sherwood number are not correctly described using Eq. (7) because the evaporation is more important after bubble departure for larger temperature. The use of Eq. (24) for the determination of the Sherwood number needs the determination of the temperature difference $\Delta T \quad \langle T_L \rangle \quad T_L^l$ responsible of the phase change at the interface. Since we can not measure this value in the experiments, we estimate the value of ΔT from the diameter evolution.

For this estimation we first consider that the Sherwood number follows Eq. (20). Secondly, to estimate the Jakob number and the corresponding overheat ΔT, a description of the evolution of the Nusselt number for growing bubble under phase change is required. Using the relation of Scriven [55] or its approximation given by Labuntsov et al. [56], it is easy to show that for our experimental conditions (evaporation in a bubble filled with a non condensible gas), the Jakob number is small ($Ja < 0.05$) so that the heat transfer is controled by the heat difussion/advection at the gas/liquid interface and not impat by the bubble volume expansion due to phase change. The Nusselt number is then given by the correlation proposed by Ruckenstein [57]

$$N_u \quad \frac{2}{\sqrt{\pi}} Pe^{th\,1/2} \tag{25}$$

where $Pe^{th} \quad RePr_L$ is the thermal Peclet number reported in Table 1. For experiment at $T \quad 30\,^\circ\mathrm{C}$, the thermal Peclet number is close to $Pe^{th} \approx 250$ during the bubble rise which corresponds to a Nusselt number of $N_u \approx 18$ (Eq. (25)). With this value, as reported in Fig. 12, Eq. (24) matches experimental measurements for a Jakob number of $Ja \quad 0.006$ and a corresponding superheat of $\Delta T \quad 0.1\,^\circ\mathrm{C}$. This estimation of the induced superheat seems to be realistic.

Note that the bubble trajectory equation (Eq. (11)) is not modified because the effect of evaporation is already taken into account through the bubble volume variation.

6. Conclusion

In this work, we have considered the mass transfer of a single nearly spherical bubble in presence of a volatile liquid phase. The nitrogen cyclohexane gas liquid system was chosen with a pressurized set up at $P \quad 20$ bar under four different operating temperatures $T \quad 30 \quad 50 \quad 100 \quad 150\,^\circ\mathrm{C}$. Bubbles of pure nitrogen were formed and released in a vessel filled with cyclohexane. In a first part, the bubble dynamic has revealed that the gas liquid system was clean. After the phase of acceleration, a quasi static evolution was observed and drag coefficient was found to be described by the drag coefficient for spherical or weakly deformed bubbles [13,49].

In a second part, by assuming that bubbles were vapor saturated at departure, the Sherwood number considering an isothermal mass transfer were presented and compared to literature correlations for a clean bubble. This approach is similar to the one previously used by Takemura and Yabe [17] for the measurement of mass transfer from oxygen spherical bubbles in silicon oil at ambient temperature. For experiments with hot liquid ($T \quad 50, 100, 150\,^\circ\mathrm{C}$) a fairly good agreement was found with correlations dedicated to mass transfer at finite Reynolds number [19,17,20]. However for experiments near the ambient temperature ($T \quad 30\,^\circ\mathrm{C}$) the measured Sherwood number appears to be around 50% lower than the predicted values from isothermal relations. This discrepancy resulted from a lower bubble volume decrease during mass transfer. This discrepancy was attributed to bubble not vapor saturated at departure. The bubble volume is then considered to be controlled by both the gas/liquid transfer of noncondensible nitrogen (bubble volume decrease) and the liquid/gas transfer due to the phase change of liquid cyclohexane (bubble volume increase). From the diameter evolution the Jakob number was estimated to be $Ja \approx 0.006$ corresponding to an interface superheat of $\Delta T \approx 0.1^\circ$. This results on the importance to consider the effect of liquid evaporation during the transfer for low Lewis number. For example, considering nitrogen as solute with other fluids of interest in hydrocarbons liquid phase oxidation like p xylene ($Le(30 \quad 150\,^\circ\mathrm{C}) \quad 60 \quad 10$), cumene ($Le(30 \quad 150\,^\circ\mathrm{C}) \quad 66 \quad 14$) or toluene ($Le(30 \quad 150\,^\circ\mathrm{C}) \quad 39 \quad 8$), the Lewis number also decrease very quickly with the temperature with a dependence on the variation of the liquid viscosity as $Le \propto \mu_L$ and the thermal diffusivity also evolves quite linearly with the temperature ($D^{th_L} \propto T$). As a result, with those fluids usually operated in pressurized vessel a similar defect with isothermal theory may be expected at low or moderate operating temperature.

It can be thought that a similar approach (Eq. (24)) can be done to study the effect of noncondensible gas mass transfer on bubble growth under phase change for the calculation of Nusselt number.

Conflict of interest

The authors declare that there is no conflict of interest.

Acknowledgments

The authors would like to thank Rhodia, member of SOLVAY group, for supporting this work. We also thank Holger Aschenbrener and Boris Binder from ICVT, Grégory Ehses and Sébastien Cazin from IMFT for they help in adapting the experimental set up for this study and in developing image processing techniques. This research was carried out within the framework of a CIFREANRT contract in collaboration with the FERMaT federation.

References

[1] P. Rollbusch, M. Bothe, M. Becker, M. Ludwig, M. Grünewald, M. Schlüter, R. Franke, Bubble columns operated under industrially relevant conditions – current understanding of design parameters, Chem. Eng. Sci. 126 (2015) 660–678.
[2] K. Idogawa, K. Ikeda, T. Fukuda, S. Morooka, Behavior of bubbles of the air-water system in a column under high pressure, Int. Chem. Eng. (1986) 468–474.
[3] H. Letzel, J. Schouten, R. Krishna, C.M. van den Bleek, Gas holdup and mass transfer in bubble column reactors operated at elevated pressure, Chem. Eng. Sci. 54 (1999) 2237–2246.
[4] L. Han, M. Al-Dahhan, Gas-liquid mass transfer in a high pressure bubble column reactor with different sparger designs, Chem. Eng. Sci. (2007) 131–139.
[5] P. Wilkinson, A. Spek, L. van Dierendonck, Design parameters estimation for scale-up of high-pressure bubble column, AIChE J. 38 (1992) 544–554.
[6] R. Krishna, M. Urseanu, D. AJ, Gas hold-up in bubble columns: influence of alcohol addition versus operation at elevated pressures, Chem. Eng. Process. 39 (2000) 371–378.
[7] R. Schafer, C. Merten, G. Eigenberger, Bubble size distributions in a bubble column reactor under industrial conditions, Exp. Therm. Fluid Sci. 26 (2002) 595–604.
[8] U. Jordan, A. Schumpe, The gas density effect on mass transfer in bubble columns with organic liquids, Chem. Eng. Sci. 56 (2001) 6267–6272.
[9] H. Jin, D. Liu, S. Yang, G. He, Z. Guo, Z. Tong, Experimental study of oxygen mass transfer coefficient in bubble column with high temperature and high pressure, Chem. Eng. Technol. 27 (2004) 1267–1272.
[10] D. Colombet, D. Legendre, A. Cockx, P. Guiraud, F. Risso, C. Daniel, S. Galinat, Experimental study of mass transfer in a dense bubble swarm, Chem. Eng. Sci. 66 (2011) 3432–3440.
[11] D. Colombet, D. Legendre, F. Risso, A. Cockx, P. Guiraud, Dynamics and mass transfer of rising bubbles in a homogenous swarm at large gas volume fraction, J. Fluid Mech. 763 (2015) 254–285.
[12] I. Roghair, M. Van Sint Annaland, J. Kuipers, An improved front-tracking technique for the simulation of mass transfer in dense bubbly flows, Chem. Eng. Sci. 152 (2016) 351–369.
[13] R. Mei, J. Klausner, C. Lawrence, A note on the history force on a spherical bubble at finite reynolds number, Phys. Fluids 6 (1994) 418–420.
[14] L. Schiller, A. Nauman, VDI Zeits 77 (1933) 318.
[15] R. Higbie, The rate of absorption of a pure gas into a still liquid during short periods of exposure, Trans. Am. Inst. Chem. Eng. 31 (1935) 365–389.
[16] J. Boussinesq, Calcul du pouvoir refroidissant des courants fluides, J. Math. Pures Appl. 6 (1905) 285–332.
[17] F. Takemura, A. Yabe, Gas dissolution process of spherical rising bubbles, Chem. Eng. Sci. 53 (1998) 2691–2699.
[18] B. Figueroa, D. Legendre, Mass or heat transfer from spheroidal gas bubbles rising through a stationary liquid, Chem. Eng. Sci. 65 (2010) 6296–6309.
[19] S. Winnikow, Letters to the editor, Chem. Eng. Sci. 22 (1967) 22–477.
[20] D. Colombet, D. Legendre, A. Cockx, P. Guiraud, Mass or heat transfer inside a spherical gas bubble at low to moderate Reynolds number, Int. J. Heat Mass Transf. 67 (2013) 1096–1105.
[21] N. Frossling, Beitr. Geophys. 32 (1938) 170.
[22] W. Ranz, W. Marshall, Evaporation from drops, Chem. Eng. Prog. 48 (4) (1952) 173.
[23] R. Clift, J. Grace, M. Weber, Bubles, Drops and Particules, Academic Press, San Diego, 1978.
[24] B. Cuenot, J. Magnaudet, B. Spennato, The effects of slightly soluble surfactants on the flow around a spherical bubble, J. Fluid Mech. 339 (1997) 25–53.
[25] F. Takemura, A. Yabe, Rising speed and dissolution rate of a carbon dioxide bubble in slightly contaminated water, J. Fluid Mech. 378 (1999) 319–333.
[26] A. Dani, A. Cockx, P. Guiraud, Direct numerical simulation of mass transfer from spherical bubbles: the effect of interface contamination at low Reynolds numbers, Int. J. Chem. React. Eng. 4 (1) (2006).
[27] S. Sadhal, R. Johnson, Stokes flow past bubbles and drops partially coated with thin films. Part 1: Stagnant cap of surfactant film-exact solution, J. Fluids Mech. 126 (1983) 237–250.
[28] W. McAdams, W. Kennel, C. Minden, R. Carl, P. Picornell, J. Dew, Heat transfer at high rates to water with surface boiling, Ind. Eng. Chem. 41 (9) (1949) 1945–1953.
[29] H. Muller-Steinhagen, N. Epstein, A. Watkinson, Effect of dissolved gases on subcooled flow boiling heat transfer, Chem. Eng. Process. 23 (1988) 115–124.
[30] K. Rainey, S. You, S. Lee, Effect of pressure, subcooling, and dissolved gas on pool boiling heat transfer from microporous, square pin-finned surfaces in FC-72, Int. J. Heat Mass Transf. 46 (2003) 23–35.
[31] P. Payvar, Mass transfer-controlled bubble growth during rapid decompression of a liquid, Int. J. Heat Mass Transf. 30 (4) (1987) 699–706.
[32] C. Bisperink, A. Prins, Bubble growth in carbonated liquids, Colloids Surf. A 85 (1994) 237–253.
[33] N. Divinis, T. Karapantsios, M. Kostoglou, C. Panoutsos, V. Bontozoglou, A. Michels, M. Sneep, R. De Bruijn, H. Lotz, Bubbles growing in supersaturated solutions at reduced gravity, AIChE J. 50 (10) (2004) 2369–2382.
[34] R. Schafer, C. Merten, G. Eigenberger, Autocatalytic cyclohexane oxidation in a bubble column reactor, Can. J. Chem. Eng. 81 (3–4) (2003) 741–748.
[35] O. Borchers, G. Eigenberger, Particle tracking velocimetry for simultaneous investigation of liquid and gas phase in bubbly flow, in: 9th International Symposium on Flow Visualization, Edinburgh, 2000.
[36] E. Bouche, V. Roig, F. Risso, A. Billet, Homogeneous swarm of high-reynolds-number bubbles rising within a thin gap. Part 1: Bubble dynamics, J. Fluid Mech. 704 (2012) 211–231.
[37] P. Marmottant, E. Villermaux, On spray formation, J. Fluid Mech. 498 (2004) 73–111.
[38] T. Maxworthy, C. Gnann, M. Kurten, F. Durst, Experiment on the rise of air bubbles in clean viscous liquids, J. Fluid. Mech. 321 (1996) 421–441.
[39] J. Vasconcelos, S. Orvalho, S. Alves, Gas-liquid mass transfer to single bubbles effect of surface contamination, AIChE J. 48 (2002) 1145–1154.
[40] D. Lynch, O. Potter, Determination of nitrogen diffusivkies in liquid cyclohexane over a wide temperature range, Chem. Eng. J. 15 (1978) 197–208.
[41] A. Einstein, On the movement of small particles suspended in stationary liquids required by the molecular-kinetic theory of heat, Ann. Phys. 17 (1905) 549–560.
[42] C. Wilke, P. Chang, Correlation of diffusion coefficient in dilute solutions, AIChE J. (1955) 264–270.
[43] J. Jonas, D. Hasha, S. Huang, Density effects on transport properties in liquid cyclohexane, J. Phys. Chem. 84 (1980) 109–112.
[44] D. Legendre, R. Zenit, J. Velez-Cordero, On the deformation of gas bubbles in liquids, Phys. Fluids 24 (2012) 043303.
[45] V. Levich, Physicochemical Hydrodynamics, Prentice-Hall, Englewood Cliffs, NJ.
[46] D. Legendre, J. Borée, J. Magnaudet, Thermal and dynamic evolution of a spherical bubble moving steadily in a superheated or subcooled liquid, Phys. Fluids 10 (6) (1998) 1256.
[47] J. Magnaudet, I. Eames, The motion of high-Reynolds-number bubbles in homogeneous flows, Annu. Rev. Fluid Mech. 32 (2000) 659–708.
[48] J. Magnaudet, D. Legendre, The viscous drag force on a spherical bubble with a time-dependent radius, Phys. Fluids 10 (1998) 550–554.
[49] D. Moore, The velocity rise of distorted gas bubbles in a liquid of small viscosity, J. Fluid Mech. 23 (1965) 749–766.
[50] H. Lamb, Hydrodynamics, 6th ed., Cambridge University Press.
[51] A. Dani, Transfert de masse entre une bulle et un liquide: simulations numeriques directes et fluorescence induite par nappe laser, Ph.D. thesis, Toulouse University, INSA Toulouse, France, 2007.
[52] D. Moore, The boundary layer on a spherical gas bubble, J. Fluid Mech. 16 (1963) 161–176.
[53] D. Legendre, On the relation between the drag and the vorticity produced on a clean bubble, Phys. Fluids 19 (2007) 018102.
[54] M. Plesset, S. Zwick, The growth of vapour bubbles in superheated liquids, J. Appl. Phys. 25 (1954) 493–500.
[55] L. Scriven, On the dynamics of phase growth, Chem. Eng. Sci. 1 (1959) 1–13.
[56] D. Labuntsov, B. Kol'chugin, V. Golovin, E. Zakharova, L. Vladimirova, Investigation of bubble growth in boiling saturated water by high-speed photography for a wide range of variation of the pressure, Teplofiz. Vys. Temp. 2 (3) (1964) 446–453.
[57] E. Ruckenstein, On heat transfer between vapour bubbles in motion and the boiling liquid from which they are generated, Chem. Eng. Sci. 10 (1959) 22.